PHYSICAL REVIEW A VOLUME 12, NUMBER 1 JULY 1975

Photoabsorption of the neutral sodium atom: A many-body calculation*

Jwei-Jun Chang and Hugh P. Kelly
Department of Physics, University of Virginia, Charlottesville, Virginia 22901
(Received 11 July 1974)

By applying many-body perturbation theory, the effects of electron correlations are included in the calculation for the photoionization cross section of the neutral sodium atom from threshold to 16 eV for the photoejected electron energy. The improvement of the lowest-order Hartree-Fock approximation for the cross section by the first-order and second-order correlation corrections is small. The discrepancy between the experiment and the calculations at the short-wavelength side of the minimum is still not understood.

I. INTRODUCTION

The alkali-metal atoms with a single valence electron outside a core would appear to be particularly simple for photoionization calculations. However, for the photoionization cross section of atomic sodium, all previous calculations[1-6] are in reasonable agreement near threshold but disagree with experiment[7] by approximately a factor of 2 at the short-wavelength side of the minimum. An excellent review of photoionization of the alkalis has been given by McDowell.[8] In this paper, we attempt to include electron correlations starting from first principles in order to discover if possible the reason for the lack of agreement between theory and experiment. We use the many-body perturbation theory of Brueckner[9] and Goldstone[10] (BG) to calculate the photoionization cross section of the ^2S ground state of the neutral sodium atom. In a previous paper, we have reported relativistic Hartree-Fock (HF) calculations for photoionization cross sections and the spin orientation of photoejected electrons from potassium, rubidium, and cesium atoms.[11] With a view to extension of the many-body perturbation theory to these higher alkali-metals in mind, we have used relativistic single-particle states in the calculation for sodium, in addition to using nonrelativistic single-particle states. Not surprisingly, the lowest-order HF results of cross sections are nearly the same, when using these two kinds of states. We have used both relativistic and nonrelativistic single-particle states for zero and first-order terms in electron correlations. The contributions from terms which are second-order in electron correlations were calculated with nonrelativistic states. In order to make certain types of higher-order diagrams become zero, as will be described in Sec. III, we choose a particular potential for computing nonrelativistic excited d states.

Our methods for applying the BG theory to the photoionization cross section of the atom have been discussed previously.[12,13] In Sec. II, we review the theory in terms of the linear response function. Section III contains results. Section IV contains discussion and conclusions.

II. THEORY

The photoionization cross section[15] σ for an atomic system is given by

$$\sigma = W/j\ , \tag{1}$$

where j is the incoming photon flux density, and W is the rate of the electron transition probability. By using the Golden rule, W is expressed as

$$W = \frac{2\pi}{\hbar}\frac{1}{l}\sum_{i,f}|\langle\Psi_f|\hat{o}|\Psi_i\rangle|^2\delta(\omega - E_f + E_i)\ , \tag{2}$$

where we take

$$\hat{o} = \sum_k \frac{l}{mc}\vec{A}\cdot\vec{P}_k$$

for the interaction between the photon and all the electrons of the atom in the nonrelativistic case and

$$\hat{o} = \sum_k e\vec{\alpha}_k\cdot\vec{A}$$

in the relativistic case.[11] We sum over all possible final states and take an average over the l degenerate initial states. The δ function refers to the transitions to higher states in which the photon energy ω (in atomic units) is absorbed. The function Ψ_i and Ψ_f are exact wave functions of the atom with energies E_i and E_f, respectively. The term $e^{i\vec{K}\cdot\vec{r}}$ in the vector potential $\vec{A}$ is replaced by unity in the dipole approximation. From

$$\delta(\omega - E_f + E_i) = \frac{1}{\pi}\mathrm{Re}\int_0^\infty ds\, e^{i(\omega - E_f + E_i)s} \tag{3}$$

we obtain

$$
\begin{aligned}
W &= \frac{2\pi}{\hbar}\,\frac{1}{\pi l}\,\mathrm{Re}\int_0^\infty ds\, e^{i\omega s} \sum_{i,f} \langle \Psi_i | e^{iE_i s}\, \hat{o}^+ e^{-iE_f s} |\Psi_f\rangle \\
&\qquad \times \langle \Psi_f | \hat{o} | \Psi_i\rangle , \\
&= \frac{2\pi}{\hbar}\,\frac{1}{\pi l}\,\mathrm{Re}\int_0^\infty ds\, e^{i\omega s} \sum_i \langle \Psi_i | \hat{o}^+(s)\hat{o}(0) | \Psi_i\rangle ,
\end{aligned}
\tag{4}
$$

where $\hat{o}^+(s) = e^{iHs}\,\hat{o}e^{-iHs}$ is a Heisenberg operator. The total Hamiltonian H for the atom is composed of an unperturbed part H_0 and a perturbation H_1, i.e., $H = H_0 + H_1$. The matrix element $\langle \Psi_i | \hat{o}^+(s)\hat{o}(0) | \Psi_i\rangle$ in (4) is the time-ordered product of two Heisenberg operators, averaged over the initial state of the atom. We have assumed that Ψ_i is a normalized wave function. If Ψ_i is an unnormalized wave function, we divide by $\langle \Psi_i | \Psi_i\rangle$ and evaluate the matrix element in the interaction picture[16] as

$$
\begin{aligned}
\frac{\langle \Psi_i | \hat{o}^+(s)\hat{o}(0) | \Psi_i\rangle}{\langle \Psi_i | \Psi_i\rangle}
&= \frac{\langle \Phi_0 | U(\infty, s)\tilde{o}^+(s)U(s,0)\tilde{o}(0)U(0,-\infty) | \Phi_0\rangle}{\langle \Phi_0 | U(+\infty, -\infty) | \Phi_0\rangle} , \\
&= \langle \Phi_0 | U(\infty, s)\tilde{o}^+(s)U(s,0)\tilde{o}(0)U(0,-\infty) | \Phi_0\rangle_L ,
\end{aligned}
\tag{5}
$$

where $\tilde{o}^+(s) = e^{iH_0 s}\,\hat{o}^+ e^{-iH_0 s}$, U is the time-evolution operator, and L indicates that the summation is over the linked terms only.[14] If we assume that the initial state is the ground state of the alkali atom, then Φ_0 is a determinant for the solution of H_0, when we choose H_0 as a sum of single-particle Hamiltonians. We express W as a sum of diagrams which are the same as the diagrams derived from the imaginary part of the frequency-dependent polarizability.[13]

The lowest-order diagram is Fig. 1(a). The diagrams with one H_1 interaction are shown by Fig. 1(b)–(e) and include their inverted diagrams. Some of the diagrams with two H_1 interactions are shown by Fig. 2(a)–(e).

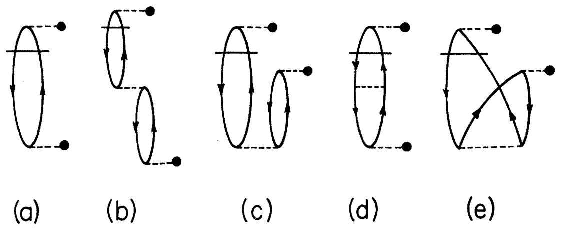

FIG. 1. Diagrams which are zero, and first-order contribution to photoionization cross section. The horizontal line indicates that the denominator contribution is treated by $-i\pi\delta$. The solid dot indicates a photon operator.

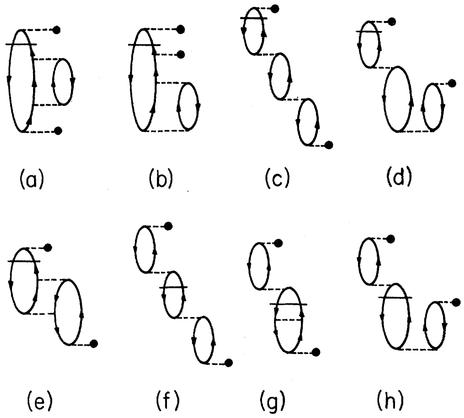

FIG. 2. Some second-order diagrams. Each diagram has two Coulomb interactions.

Each diagram has two heavy dots and an odd number of horizontal lines. The upper dot refers to $\tilde{o}^+$ and the lower one to $\tilde{o}$. Since denominators D can vanish, they are replaced by $D + i\eta$.[13] The horizontal line indicates that the imaginary part is taken from the right-hand side of the equation $(D + i\eta)^{-1} = \mathrm{P}D - i\pi\delta(D)$, where P represents a principal-value integration.

When the diagram has only one horizontal line, we may well only consider the part either below or above the horizontal line. In such a way, many more higher-order diagrams will be included by adding the parts below the horizontal line and squaring the sum. For instance, the diagrams Fig. 2(f)–(h) and many others may be included by adding the diagrams Fig. 3(a)–(e) and then squaring the sum.

III. RESULTS

In order to calculate the diagrams, it is necessary to obtain a complete set of single-particle states for each orbital angular momentum.

In the nonrelativistic case, the s states were computed from the Hartree-Fock (HF) $3s$ equation. The p states are calculated with a Silverstone-Huzinaga[17,18] potential by removing the $3s$ electron so that the $2p$ orbital is the HF $2p$ orbital, and

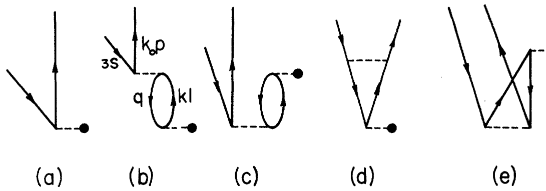

FIG. 3. Open diagrams corresponding to diagrams in Fig. 1, by taking the parts below the horizontal lines.

excited p states have the property of being computed in the field of the $(1s)^2(2p)^6$ core. The equation satisfied by the excited np radial wave function P_{np} becomes

$$\left(-\frac{1}{2}\frac{d^2}{dr^2}-\frac{11}{r}+\frac{6}{r^2}+(2J^0_{1s}-\tfrac{1}{3}K^0_{1s})+(2J^0_{2s}-\tfrac{1}{3}K^0_{2s}) + (6J^0_{2p}-K^0_{2p})-\tfrac{2}{5}K^2_{2p}\right)P_{np} + \langle 2p|J^0_{3s}-\tfrac{1}{6}K^1_{3s}|np\rangle P_{2p}=\epsilon_{np}P_{np}, \tag{6}$$

where J^K_{nl} and K^K_{nl} are defined as

$$J^K_{nl}P_i(r)=\int_0^\infty dr'(r^K_</r^{K+1}_>)P^*_{nl}(r')P_{nl}(r')P_i(r), \tag{7}$$

$$K^K_{nl}P_i(r)=\int_0^\infty dr'(r^K_</r^{K+1}_>)P^*_{nl}(r')P_i(r')P_{nl}(r), \tag{8}$$

and $r_<$ ($r_>$) is the smaller (larger) of r and r'.

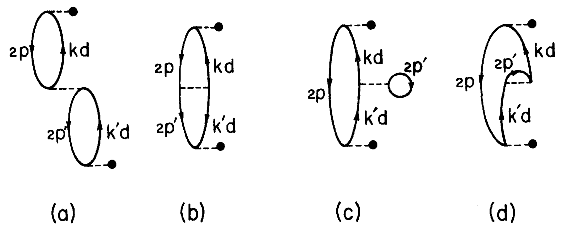

FIG. 4. The diagrams used to obtain the part of potential referring to six $2p$ electrons for computing excited d states.

The potential for d states is chosen from the field of the nucleus, two $1s$ electrons, two $2s$ electrons, one $3s$ electron, but the part for six $2p$ electrons is obtained by setting the sum of the diagrams Fig. 4(a)–(d) to zero. With this potential for d states, the sum of the diagrams Fig. 5(a)–(d) may become zero,[19,20] and so is the sum of the similar higher-order diagrams. Then the equation for the radial wave function P_{nd} is written

$$\left(-\frac{1}{2}\frac{d^2}{dr^2}-\frac{11}{r}+\frac{6}{r^2}+\left[(2J^0_{1s}-\tfrac{1}{5}K^2_{1s}) + (2J^0_{2s}-\tfrac{1}{5}K^2_{2s})+(5J^0_{2p}-\tfrac{1}{5}J^2_{2p}+\tfrac{14}{15}K^1_{2p}-\tfrac{9}{35}K^3_{2p}) + (J^0_{3s}-\tfrac{1}{10}K^2_{3s})\right]\right)P_{nd}=\epsilon_{nd}P_{nd}. \tag{9}$$

In the relativistic case, the s-$\frac{1}{2}$ states are computed from the Dirac-Hartree-Fock (DHF) $3s_{1/2}$ equation, and the $\overline{p}_{1/2}$ states and $p_{3/2}$ states are computed from the DHF equations by removing the $3s$ electron. The excited $\underline{d}_{3/2}$ states and $d_{5/2}$ states are computed in the field of the atom with a $2\overline{p}_{1/2}$ electron missing and with a $2p_{3/2}$ electron missing, respectively. For example, the equations for the $d_{5/2}$ states are

$$\begin{aligned}&\frac{dP_{nd}}{dr}-\frac{3}{r}P_{nd}+\left\{2c+\frac{1}{c}\left[\frac{Y(nd;r)}{r}-\epsilon_{nd}\right]\right\}Q_{nd}+W_Q(nd;r)=0,\\ &\frac{dQ_{nd}}{dr}+\frac{3}{r}Q_{nd}+\frac{1}{c}\left[\frac{Y(nd;r)}{r}-\epsilon_{nd}\right]P_{nd}-W_p(nd;r)=0,\end{aligned} \tag{10}$$

where

$$Y(nd;r)=11-2Y_0(1s,1s;r)-2Y_0(2s,2s;r)-2Y_0(2\overline{p},2\overline{p};r)-3Y_0(2p,2p;r)+\tfrac{3}{175}Y_2(2p,2p;r)-Y_0(3s,3s;r), \tag{11}$$

$$W_{P\text{ or }Q}(nd;r)=-\frac{1}{rc}\{\tfrac{1}{5}Y_2(nd,1s;r)[P_{1s}\text{ or }Q_{1s}]+\tfrac{1}{5}Y_2(nd;2s;r)[P_{2s}\text{ or }Q_{2s}]+\tfrac{1}{7}Y_3(nd,2\overline{p};r)[P_{2\overline{p}}\text{ or }Q_{2\overline{p}}] + [\tfrac{1}{5}Y_1(nd,2p;r)+\tfrac{22}{245}Y_3(nd;2p;r)][P_{2p}\text{ or }Q_{2p}]+\tfrac{1}{10}Y_2(nd,3s;r)[P_{3s}\text{ or }Q_{3s}]\}, \tag{12}$$

and

$$Y_K(A,B;r)=r\int_0^\infty\frac{r^K_<}{r^{K+1}_>}[P_A(r')P_B(r')+Q_A(r')Q_B(r')]\,dr'. \tag{13}$$

In our calculation, we may choose the incoming photon as linearly polarized or as circularly polarized. We have assumed the photon linearly polarized along the $\hat{Z}$ axis for the nonrelativistic case so that there is an operator ∇_0 (or an operator Z for the length form) in the photon operator $\hat{o}$, but we have assumed right-circularly polarized photons for the relativistic case so that there is an operator α_+ in the photon operator $\hat{o}$.

Our lowest-order cross sections calculated

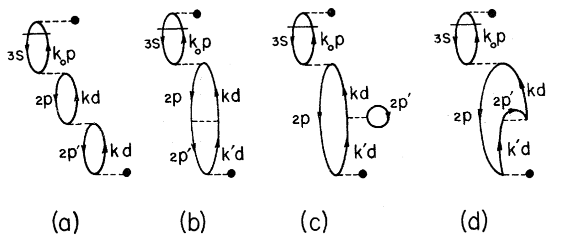

FIG. 5. The diagrams having zero contributions, because we used the potential as mentioned in Fig. 4.

from the nonrelativistic single-particle states by using both the velocity form and the length form, are compared with that computed from the relativistic single-particle states in Table I. These results are essentially the same as the HF results of Seaton.[1]

Over the energy range which we calculated, the denominator in the diagram Fig. 3(b) never vanishes. The matrix element of diagram Fig. 3(b) with $q = 2p$, $kl = kd$ is about ten times larger than that with $q = 2p$, $kl = ks$, where k refers to the particle line and l to the angular momentum. When the velocity form is used, the magnitudes of matrix elements for the first-order diagram Fig. 3(b) and 3(c) are sometimes as large as the lowest-order diagram Fig. 3(a), but they are opposite in sign so that there is a large cancellation between diagrams 3(b) and 3(c). The sum of them contributes about one-tenth of the lowest-order results. The other diagrams Fig. 3(d) and (e) in the first order are small when compared with the diagrams Fig. 3(b) and (c).

In diagram Fig. 3(b) with $q = 2p$, $kl = ks$, the core electron state $2p_0^-$ can be excited into the $3s^-$ state, whereas the core electron state $2p_0^+$ is prohibited from doing this as the $3s^+$ is an unexcited state.

TABLE I. Lowest-order contributions.

K [a] (a.u.)	σ_{0L} [b] (10^{-20} cm^2)	σ_{0V} [c] (10^{-20} cm^2)	σ_{0R} [d] (10^{-20} cm^2)
0.1	6.612	4.976	5.307
0.2	1.632	0.963	1.033
0.3	0.058	0.299	0.234
0.4	2.375	3.318	3.234
0.5	5.933	7.222	7.033
0.6	8.622	9.992	9.766
0.7	9.875	11.151	11.239
0.8	9.959	11.061	11.334
0.9	9.339	10.249	10.190
1.0	8.411	9.127	9.194
1.1	7.395	7.947	7.892
1.2	6.435	6.839	6.800

[a] The ejected electron momentum K.
[b] Nonrelativistic results using the length form.
[c] Nonrelativistic results using the velocity form.
[d] Relativistic results.

Using the velocity form for nonrelativistic single-particle states, the matrix element of the lowest-order diagram changes sign near the energy 0.034 a.u. for the photoejected electrons and causes a zero minimum of cross section. The matrix elements of the first-order diagrams of Fig. 3(b)–(e), however, do not change sign around the minimum and this minimum shifts from the energy 0.034 to 0.032 a.u. for the photoejected electrons.

For relativistic single-particle states, $\langle p_{1/2,\,1/2}|\alpha_+|s_{1/2,\,-1/2}\rangle$ and $\langle p_{3/2,\,1/2}|\alpha_+|s_{1/2,\,-1/2}\rangle$ or $\langle p_{3/2,\,3/2}|\alpha_+|s_{1/2,\,1/2}\rangle$ come to zero at different energies. This results in a nonzero minimum photoionization cross section. Our estimated nonzero minimum photoionization cross section by including first-order correction is 4×10^{-24} cm^2 as compared with 9×10^{-24} cm^2 calculated by Weisheit.[6]

For both the nonrelativistic cases, the cross-section curve from the lowest-order contribution is brought down near threshold by adding the contribution from the first-order terms, but is pushed up at the short-wavelength side of the minimum. The results of adding the diagrams of Fig. 3(a)–(e) and then squaring the sum are shown in Table II. We note that nonrelativistic results including first-order correlations are quite similar for both ve-

TABLE II. Photoionization cross section for sodium including correlation effects.

K (a.u.)	σ_{1L} [a] (10^{-20} cm^2)	σ_{1V} [b] (10^{-20} cm^2)	σ_{1R} [c] (10^{-20} cm^2)	σ [d] (10^{-20} cm^2)
0.1	4.759	4.634	3.583	2.309
0.2	0.785	0.733	0.345	0.413
0.3	0.401	0.424	0.897	0.363
0.4	3.714	3.689	5.190	2.972
0.5	7.954	7.950	10.001	6.655
0.6	11.039	11.169	13.369	10.051
0.7	12.408	12.508	15.200	12.133
0.8	12.428	12.474	15.411	13.119
0.9	11.608	11.500	14.120	12.709
1.0	10.409	10.185	12.992	11.413
1.1	9.050	8.668	11.483	9.931
1.2	7.759	7.307	10.217	9.148

[a] Nonrelativistic results obtained by adding the diagrams of Fig. 3(a)–(e) and squaring the sum. The length form was used for dipole matrix elements.
[b] Nonrelativistic results obtained from the diagrams of Fig. 3(a)–(e) with the velocity form.
[c] Relativistic results obtained from the diagrams of Fig. 3(a)–(e).
[d] Final nonrelativistic results obtained by adding Fig. 3(a)–(e), Fig. 6(a)–(f), and Fig. 7(a)–(j), and then squaring the sum with use of the velocity form.

locity and length matrix elements, although they are different in the lowest order. Of course, the cross sections should be the same for both the velocity form and the length form if the exact wave functions for Ψ_i and Ψ_f are used in Eq. (2).

We have also included matrix-element contributions which are second-order in H' as shown in Fig. 6. We found that the main contributions are from the diagrams of Fig. 6(a) with $q = 2p$, $k_2l_2 = k_2p, k_3l_3 = k_3p$ and with $q = 2p$, $k_2l_2 = k_2d$, $k_3l_3 = k_3d$ and from the diagram of Fig. 6(e) with $q = 2p$, $kl = kd$. The exchange diagram Fig. 6(b) is small as compared with the diagram Fig. 6(a). For example, the diagram Fig. 6(b) with $q = 2p$, $k_2l_2 = k_2d$, $k_3l_3 = k_3d$ has the same radial part integration as the diagram Fig. 6(a) with $q = 2p$, $k_2l_2 = k_2d$, $k_3l_3 = k_3d$, but the former has an angular factor 0.044 444 from the two Coulomb interactions by summing over the magnetic quantum numbers and the latter has an angular factor 0.888 888.

The diagrams of Fig. 6(a), (b), and (e) are the first ones to have denominators with singularities and were calculated by taking the principal value. But denominators for the diagrams Fig. 6(c), (d), and (f) do not vanish.

The diagram of Fig. 6(c) represents initial-state correlation, since the $3s^+$ hole line is excited to the particle line k_3l_3 through two Coulomb interactions with the core-electron hole line q before the interaction with the photon. We note that the diagram exists only when the particle line k_3l_3 is the k_3s state so that total angular momentum is conserved for the ground-state configuration. For the photon interaction matrix $\langle k_0p|\hat{o}|k_3s\rangle$, we have to deal with the continuum wave function k_3s transition to the continuum wave function k_0p. Since the continuum wave functions become sinusoidal in the asymptotic region, the value of $\langle k_0p|\hat{o}|ks\rangle$ involves integration to infinity. But, from the fact that the photon is only absorbed within the atom, we expect to be able to use a cutoff. We have chosen cutoffs such that radial part of the 3s wave function becomes zero to 10^{-3} or 10^{-6}, i.e., around 15 a_0 or 30 a_0 from the origin, respectively. We note that the matrix elements $\langle k_0p|\hat{o}|k_3s\rangle$ peak sharply (and are ∞) at $k_0 = k_3$, but the integration over k_3 should converge. We found that the triple integration over k_1, k_2, and k_3 for the diagram 6(c) is approximately invariant with respect to the cutoff radii of 15 a_0 or 30 a_0, although the $\langle k_0p|\hat{o}|k_3's\rangle$ matrix elements have different values using the two cutoff radii. It is often desirable to present both length and velocity results for comparison. However, in calculating diagrams with continuum to continuum dipole matrix elements such as shown in Fig. 6(c) and 6(d), it is numerically more convenient to use the dipole velocity rather than the dipole length form. This is because even when the cutoff in the radial integration is used, the matrix elements $\langle k|z|k'\rangle$ and $\langle k|d/dz|k'\rangle$ are rather sharply peaked for values of k' near to k and it becomes necessary to calculate many states k'. The matrix element $\langle k|d/dz|k'\rangle$, although large for $k = k'$, is much less sharply peaked than $\langle k|z|k'\rangle$ and so a much smaller mesh can be used with the velocity operator. For convenience, then, the higher-order diagrams were calculated only with the velocity operator.

We have also explicitly calculated the diagrams of Fig. 7(a)–(j) and have found that they do not have large contributions. These contributions might be neglected, but we have included them in

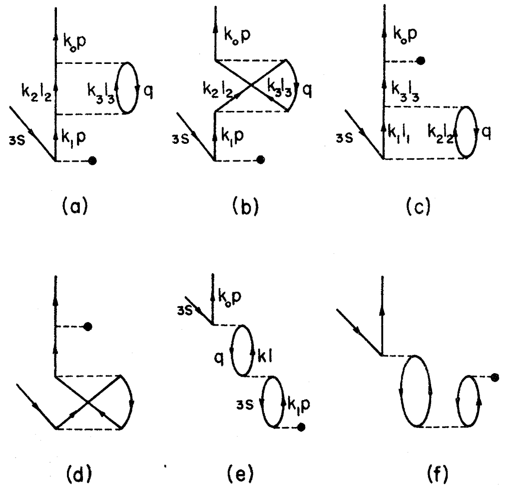

(a) (b) (c)
(d) (e) (f)

FIG. 6. The dominant second-order open diagrams.

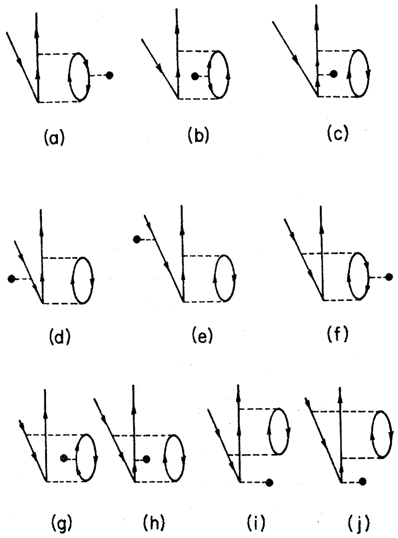
(a) (b) (c)
(d) (e) (f)
(g) (h) (i) (j)

FIG. 7. Some second-order open diagrams.

our final results which are obtained by adding the diagrams of Fig. 3(a)–(e), Fig. 6(a)–(f), and Fig. 7(a)–(j) for the velocity form, and then squaring the sum. Our total final results are shown in the last column of Table II.

IV. DISCUSSION AND CONCLUSIONS

The first accurate theoretical calculations for the photoionization cross section of sodium were the HF results obtained by Seaton.[1] As already mentioned, these calculations are essentially our lowest-order results. The nonzero minimum in the cross section is explained by including spin-orbit effects. The HF results do not agree well with experiment at the short-wavelength side of minimum. This motivated us to include correlations effects carefully, with the hope of reconciling this discrepancy. We have included first-order correlation corrections both with relativistic and nonrelativistic states. The nonrelativistic calculations were carried out with both length and velocity forms for the dipole matrix elements. All three types of calculations were in close agreement with each other, but did not differ greatly from the HF results, and so the discrepancy with experiment still remains. We also included second-order correlation effects with nonrelativistic states and the velocity form of the dipole matrix elements. The discrepancy with experiment still remains.

Recently, Weisheit[6] has calculated the photoionization cross section for sodium using a core-polarization correction to the dipole transition moment and a model potential plus the spin-orbit interaction. In Fig. 8 our results are compared with those of Weisheit and also with the experimental results of Hudson and Carter.[7] Near threshold our results are lower than those of Weisheit and not in as good agreement with experiment. Beyond the minimum in the cross section, our results are in reasonable agreement with those of Weisheit. Both calculations disagree with experiment at the short-wavelength side of minimum.

In Figs. 8 and 9 we have only presented our velocity results. In Fig. 8 we have omitted the length results because the figure would then be cluttered. However, the length and velocity results in lowest-order and with first-order Coulomb corrections are compared in Tables I and II. It is interesting that σ_{1L} and σ_{1V} in Table II are very close.

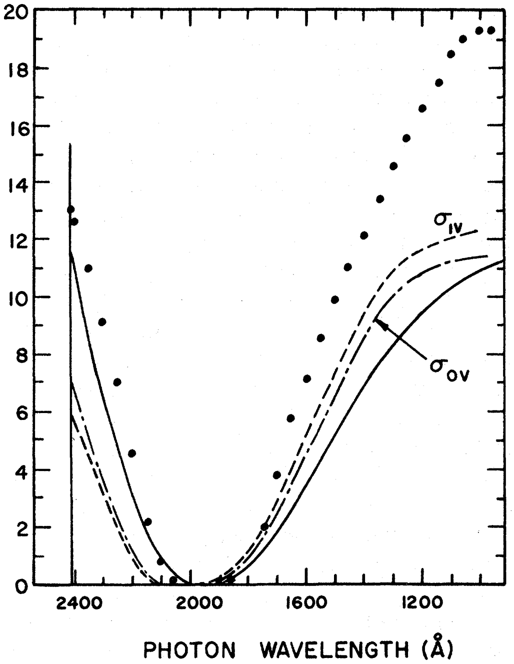

FIG. 8. Photoionization cross section of the sodium vs the energy of incoming photon. Solid line, results calculated by Weisheit (Ref. 6). Filled circles, measurements reported by Hudson and Carter (Ref. 7). σ_{0V} and σ_{1V} are our lowest- and first-order results, respectively, by using nonrelativistic single-particle states in the velocity form.

Previous calculations were also carried out by Cooper,[2] who used a simplified one-electron model based on the effective central potential obtained from HF orbitals. His results gave too low values near threshold, but had reasonable agreement with experiment from the minimum to 6 eV for the photoejected electron. Boyd[3] used a Hartree potential, modified to include polarizability effects and his results are shown in Fig. 9. Sheldon[4] used the quantum-defect method of Burgess and Seaton[5] and obtained results in excellent agreement with experiment from threshold to 6 eV for the photoejected electron, but beyond 6 eV his results

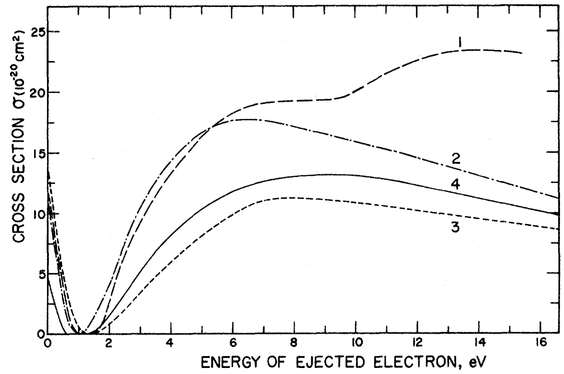

FIG. 9. Photoionization cross section of sodium vs the energy of the ejected electron. Curve 1 represents the experimental results; 2, Sheldon; 3, Boyd (dipole velocity); 4, our final results (dipole velocity).

also disagree with experiment as shown in Fig. 9. Our final results at the short-wavelength side of the minimum fall between those of Sheldon and Boyd as shown in Fig. 9. From 10 to 16 eV for the photoejected electron, all the theoretical curves decrease: Sheldon's curve from 15×10^{-20} cm^2 to 10×10^{-20} cm^2; Boyd's curve from 10×10^{-20} cm^2 to 8×10^{-20} cm^2; our curve from 12×10^{-20} cm^2 to 10×10^{-20} cm^2. However, the experimental curve increases from 20×10^{-20} cm^2 to 23×10^{-20} cm^2. This discrepancy is still unresolved, and it is not clear to us that there are important diagrams which remain to be calculated. A recent calculation by Chang[21] approximately included higher-order diagrams by use of a semiempirical polarization potential but also did not find the increase in σ at 10 eV for the ejected electron as shown in Fig. 9.

---

*Research supported by the Aerospace Research Laboratories, Office of Aerospace Research, U.S. Air Force Contract No. F33615-69-C-1048.

[1] M. J. Seaton, Proc. R. Soc. (Lond.) A 208, 418 (1951).

[2] J. W. Cooper, Phys. Rev. 128, 681 (1962).

[3] A. H. Boyd, Planetary Space Sci. 12, 729 (1964).

[4] J. W. Sheldon, J. Appl. Phys. 37, 2928 (1966).

[5] A. Burgess and M. J. Seaton, Monthly Not. R. Astron. Soc. 120, 121.

[6] J. C. Weisheit, Phys. Rev. A 5, 1621 (1972).

[7] R. D. Hudson and V. L. Carter, J. Opt. Soc. Am. 57, 651 (1967).

[8] M. R. C. McDowell, in *Case Studies in Atomic Collisions Physics 1*, edited by E. W. McDaniel and M. R. C. McDowell (North-Holland, London, 1969), p. 47.

[9] K. A. Brueckner, Phys. Rev. 97, 1353 (1955).

[10] J. Goldstone, Proc. R. Soc. (Lond.) A 239, 267 (1957).

[11] J. J. Chang and H. P. Kelly, Phys. Rev. A 5, 1713 (1972).

[12] H. P. Kelly, Phys. Rev. 136, B896 (1964).

[13] H. P. Kelly and A. Ron, Phys. Rev. A 5, 168 (1972).

[14] A. J. Glick, in The Many-Body Problem (1961 Bergen International School of Physics), edited by C. Fronsdal (unpublished); P. Longe and A. J. Glick, Phys. Rev. 177, 526 (1969).

[15] A. I. Akhiezer and V. B. Berestetsky, *Quantum Electrodynamics* (U.S. GPO, Washington, D.C., 1957), p. 313.

[16] A. L. Fetter and J. D. Walecka, *Quantum Theory of Many-Particle Systems* (McGraw-Hill, New York, 1971), p. 83.

[17] H. J. Silverstone and M. L. Yin, J. Chem. Phys. 49, 2076 (1968).

[18] S. Huzinaga and C. Arnau, Phys. Rev. A 1, 1285 (1970).

[19] M. Ya. Amus'ya, N. A. Cherepkov, and L. V. Chernysheva, Zh. Eksp. Teor. Fiz. 60, 160 (1971) [Sov. Phys. —JETP 33, 90 (1971)].

[20] T. Ishihara and R. T. Poe, Phys. Rev. A 6, 111 (1972).

[21] T. N. Chang, J. Phys. B 8, 743 (1975).